

Supplementary information: The free-energy barriers against expansion of the metastable fusion stalk and its implication for the protein fusion machinery

Herre Jelger Risselada, Gregory Bubnis, Helmut Grubmüller

Theoretical Molecular Biophysics Group, Max-Planck-Institute for Biophysical Chemistry, 37077 Göttingen, Germany,

Methods:

System setup. All vesicles were obtained by spontaneous aggregation of randomly placed lipids. This method is described in detail elsewhere [1]. An additional long equilibration run of 20 μ s was performed for the mixed lipid systems (two artificial pores were present) [2]. In all cases, equilibrium of the vesicle was defined by the flux convergence of the lipid components. The pure POPC vesicle/dimples consisted of 2217 lipids. The mixed POPC:POPE system, 1330 POPC and 887 POPE (40%) lipids. The mixed POPC:cholesterol system, 1980 POPC and 834 cholesterol (30%) molecules. The box dimensions in our (umbrella) simulations were $21 \times 22 \times 20 \text{ nm}^3$. About 50000 solvent beads were present. All vesicles were equilibrated with 2 artificial pores of 1.6 nm radius. Equilibrium is defined by the absence of net flux/flip-flops for each individual component, which can take up to 20 μ s in the mixed vesicles [2].

Artificial pores and stalk formation. The hydrophilic pore of radius $R=1.6 \text{ nm}$ was stabilized using an repulsive potential $U(r_i)$ with $U(r_i) = 1/2k(r_i - R)^2$, if $r_i < R$ and $U(r_i) = 0$ if $r_i \geq R$, where r_i denotes the (minimal) distance of the center of mass of the lipid from the pore center and k a force constant ($k_{\text{force}}=50 \text{ kJ nm}^{-2} \text{ mol}^{-1}$) [1, 2]. This potential only acts on carbon lipid tails and glycerol groups. The central axis through the pores was along the x-axis with coordinates $y=0.5 \times \text{box length}$, $z=0$. This particular choice ($z=0$) does not interfere with the scaling of coordinates due to the pressure coupling. Likewise, we induced the initial stalk in the bilayer fusion setup by applying an external field. Here, we applied the same harmonic potential to induce a $R=1.0 \text{ nm}$ 'void' in the solvent layer between the bilayers. The hydrophobic nature of the void attracts the lipid tails in the adjacent leaflets and results in the formation of a stalk. The external field was subsequently removed to allow equilibration of the stalk structure.

The membranes are defined tension-less because there is no degree of freedom that allows lateral membrane tension to built-up. The lipids can freely distribute

themselves over the monolayers via the artificial pores, i.e. the chemical potential of the monolayers are equal and there is no possibility to build up any osmotic pressure difference. Further, the simulations box is semi-isotropically coupled to independent pressure baths of 1.0 bar such that there can not be a resultant pulling or squeezing force on the stalk/vesicle coming from the boundary conditions (the simulation box).

Hydrophilic probes. A hydrophilic probe consisted of 8 P4 particles [3], which are located on the edges of a cube with a dimension of 0.3×0.3 nm. The beads were connected via 12 direct lattice bonds (0.3 nm), 12 in plane diagonal bonds (0.424 nm), and 4 diagonal bonds (0.52 nm), each with a harmonic force constant of 1250 kJ nm $^{-2}$ mol $^{-1}$.

Umbrella sampling. In umbrella sampling one attempts to overcome sampling problems along an quasi-static reaction coordinate by introducing an external bias potential such that the unfavorable free energy states are sampled adequately. To conduct umbrella sampling, one must generate a series of configurations along a reaction pathway (umbrella windows). These umbrella windows are restraint by the bias potential to sample a limited, but overlapping region of the reaction pathway. Afterward, the potential of mean force is constructed from the different umbrella windows by correcting for the introduction of the biasing potential.

Umbrella windows were obtained by performing an initial pulling simulation where the probes were pulled together at a constant rate of -5×10^{-5} nm/ps until barrier crossing. This simulation was divided in 40 to 50 different fragments with a progressing probe to probe distance, and which formed the setup for the actual production runs (i.e., umbrella simulations). The harmonic force constant of the 'bond' between the probes was 1000 kJ nm $^{-2}$ mol $^{-1}$. We note that the probes can freely translate throughout the system, and that the observed location of the probes in an outcome of the free-energy minimization of the membranes. Further, in the stalk widening simulations, we only restrained the x-dimension of the vector connecting the two probes, i.e. the dimension parallel to the central axis through the stalk. Therefore, the probes can move independently within the xy-plane which lies perpendicular to the symmetry axis of the stalk (the actual distance between the probes in 3 dimensions is irrelevant). In this way, we do not oppose radial symmetry when forcing the probes together, because the probes can penetrate the stalk at an angle. The cited probe-probe distance is the distance along the z-dimension. In the leaky stalk simulations, we only restrained the actual distance between the probes (three dimensional), and the cited probe-probe distance is the length of connecting vector. We note, however, that these bonded probes can freely move and translate within the system like a diatomic molecule. We allowed

for 400 ns of equilibration time in each umbrella window (see Fig. S10). We note that stalk expansion can be alternatively enforced by bringing two lipids in the trans-leaflet within close contact (Fig. S14), and that the obtained results are very similar. In addition, we note that 'pinching' the membrane via the probes hardly affects the nearby lipid composition in the mixed POPC:POPE membranes (Fig. S15).

Error bars were calculated using the bootstrapping method [4], where the error is estimated from differences between different sampling intervals. We used the weighted histogram method to reconstruct the potential of mean force from the different umbrella windows [4]. In our simulations we bring the system close to its barrier such that barrier crossing (nucleation) can occur within the 1.6 microsecond time-scale of the umbrella simulations. It is important that the simulations are of equal length and sufficiently short such that nucleation along the reaction coordinate becomes unlikely if the remaining free energy barrier is larger than several $k_b T$.

Bending restraint. We restrained bending of the trans-leaflet by applying position restraints on the amino beads of the lipids with a force constant of 1000 kJ nm⁻² mol⁻¹. The restraint only acted in the Z-dimension, i.e. the dimension parallel to the two probes, and allowed free movement/diffusion in the xy-plane. We re-introduced the two artificial pores, such that the lipids in the unrestrained trans-leaflets can freely flip-flop and diffuse. Further, the z-dimension, and xy-dimension of the simulation box could freely and independently adapt such that the unrestrained leaflet remains tension less.

Simulation details. The simulations described in this paper were performed with the GROMACS simulation package [6], version 4.0.5. We used the Martini model version 2.1 [3, 7] to simulate the lipids and cholesterol. In all simulations the system was coupled to a constant temperature bath [8] of 310 K with a relaxation time τ_T of 1.0 ps. The time step used in the simulation was 20 fs [9]. Shifted potentials were used to describe van der Waals and electrostatic pair-wise interactions. In both cases, the neighbor list cutoff was 1.2 nm and these potentials were gradually shifted to zero when the pair-wise distance exceeded 0.9 nm (van der Waals) or 0 nm (Coulomb interaction). The neighbor list was updated every 10 simulation steps. The pressure was semi-isotropically coupled [8] to 1 bar with a relaxation time τ_P of 0.5 ps. In analogy to the other studies employing the Martini model, time scales quoted in this work were scaled by a factor of 4 to correct for the 4-times faster diffusion rates of water and lipids in the coarse-grained model [3] with respect to reality.

References

- [1] Risselada, H, Mark, A, Marrink, S (2008) Application of mean field boundary potentials in simulations of lipid vesicles. *J. Phys. Chem. B* 112:7438–47.
- [2] Risselada, H, Marrink, S (2009) Curvature effects on lipid packing and dynamics in liposomes revealed by coarse grained molecular dynamics simulations. *Phys. Chem. Chem. Phys.* 11:2056–67.
- [3] Marrink, SJ, Risselada, HJ, Yefimov, S, Tieleman, DP, de Vries, AH (2007) The MARTINI force field: Coarse grained model for biomolecular simulations. *J. Phys. Chem. B* 111:7812–7824.
- [4] Hub, J, de Groot, B, van der Spoel, D (2010) g_wham - A free weighted histogram analysis implementation including robust error and autocorrelation estimates. *J. Chem. Theory Comput.* 6:3713–3720.
- [5] Risselada, H et al. (2012) Line-tension controlled mechanism for influenza fusion. *PLoS One* 7:e38302.
- [6] Hess, B, Kutzner, C, Van Der Spoel, D, Lindahl, E (2008) GROMACS 4: Algorithms for highly efficient, load-balanced, and scalable molecular simulation. *J. Chem. Theory Comput.* 4:435.
- [7] Monticelli, L et al. (2008) The martini coarse grained force field: Extension to proteins. *J. Chem. Theory Comput.* 4:819–834.
- [8] Berendsen, HJC, Postma, JPM, van Gunsteren, WF, Di Nola, A, Haak, JR (1984) Molecular-dynamics with coupling to an external bath. *J. Chem. Phys.* 81:3684–3690.
- [9] Marrink, SJ, Periole, X, Tieleman, DP, de Vries, AH (2010) Reply to the comment on on using a too large integration time step in molecular dynamics simulations of coarse-grained molecular models. *Phys. Chem. Chem. Phys.* 12:2257–2258.
- [10] Lee, KK (2010) Architecture of a nascent viral fusion pore. *EMBO* 29:1299–1311.

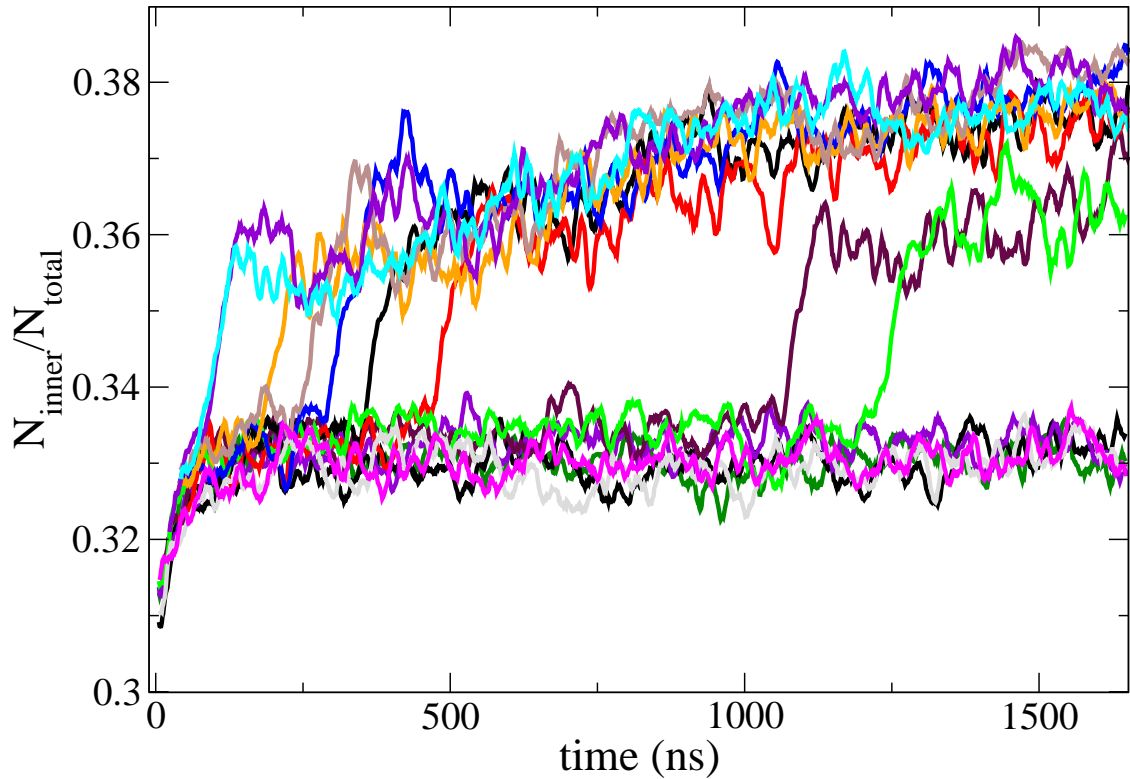


Figure 1: Lipid flip-flops for the different umbrella windows (i.e., different probe to probe distances) in the presence of artificial pores(Stalk widening, pure POPC). Shown is the relative population of the trans-leaflet N_{inner} as function of time ($N_{total} = 2217$ lipids). In these simulations we started with a vesicle obtained by spontaneous formation ($N_{inner}/N_{total} = 0.31$). The sudden transition toward higher values (> 0.33) reflect barrier crossing – subsequent widening of the stalk becomes spontaneous. In the different umbrella windows were barrier crossing is not observed N_{inner}/N_{total} remains about 0.33 (equilibrium). The latter indicates that, upto the barrier, the process of stalk widening seems not characterized by a pronounced change in relative leaflet population.

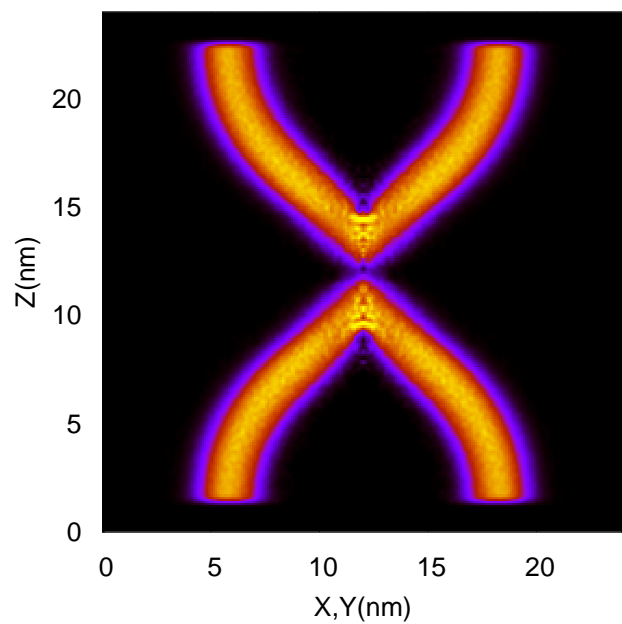
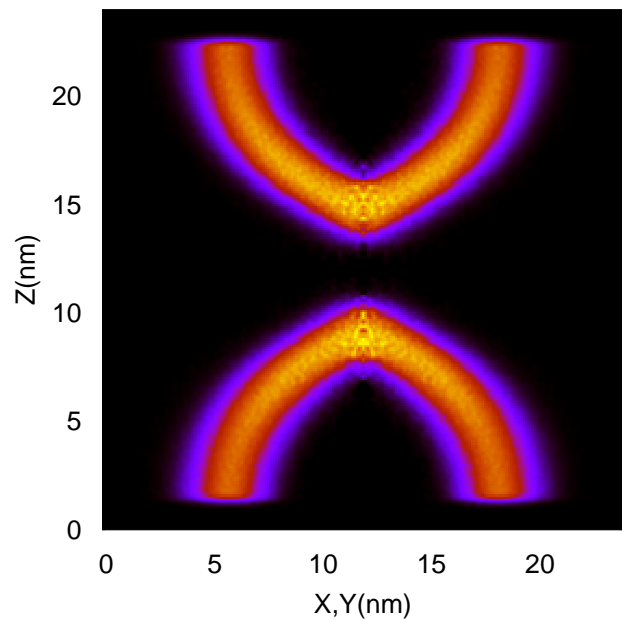


Figure 2: Stalk widening in the pure POPC membrane (equilibrated vesicle, without artificial pores). Shown are the radially averaged densities of the trans-leaflets for the relaxed stalk (*upper panel*) and the trans membrane contact (*lower panel*)

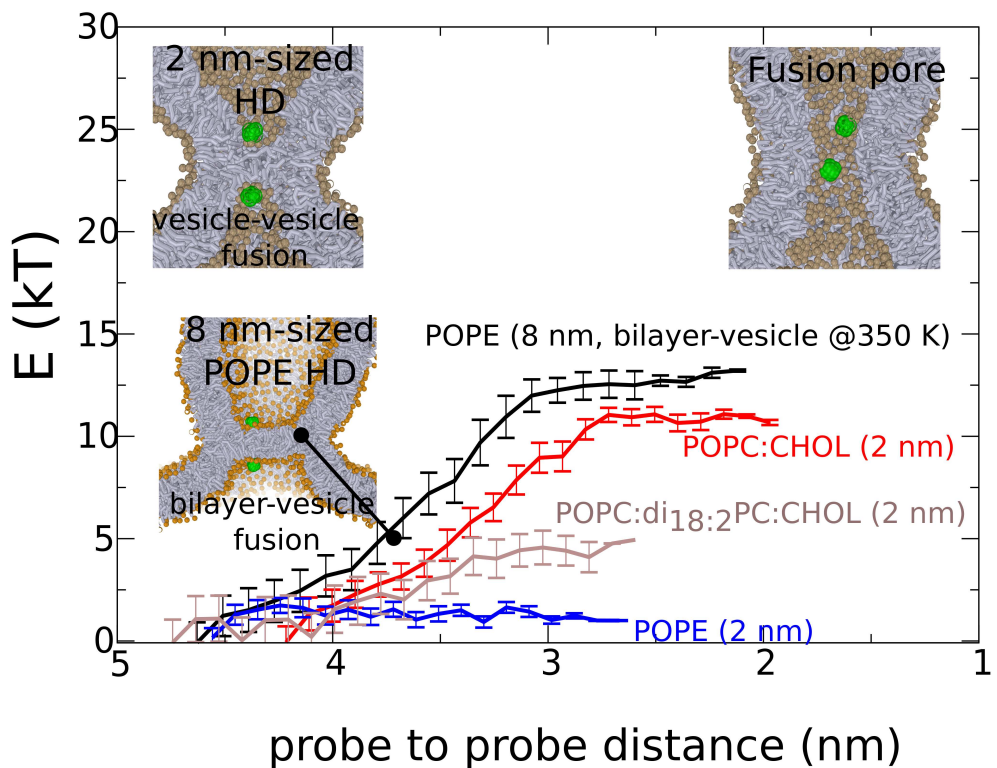


Figure 3: Free-energy barrier against subsequent rupture of the small 2nm-sized hemifusion diaphragm. Shown is the free-energy for different membrane compositions. For pure POPC, 40% POPE, or even pure POPE the barrier is within the thermal noise and spontaneous rupture events are observed in our $1.6 \mu\text{s}$ simulations. The presence of 30% cholesterol strongly increases the barrier against rupture, about $11 k_B T$. The strengthening effect of cholesterol is, however, reduced when 50% of the POPC lipids are replaced by membrane disordering poly-unsaturated lipids diC_{18:2}PC. The black line shows the barrier against pore (rim-pore) formation in an 8nm-sized hemifusion diaphragm formed between a pure POPE vesicle and 35x35 nm lipid bilayer (see Current Opinion in Structural Biology, 22(2), 187-196, 2012), about $13 k_B T$, and illustrates the dependence of the barrier on the size and topology of the hemifused membrane structure.

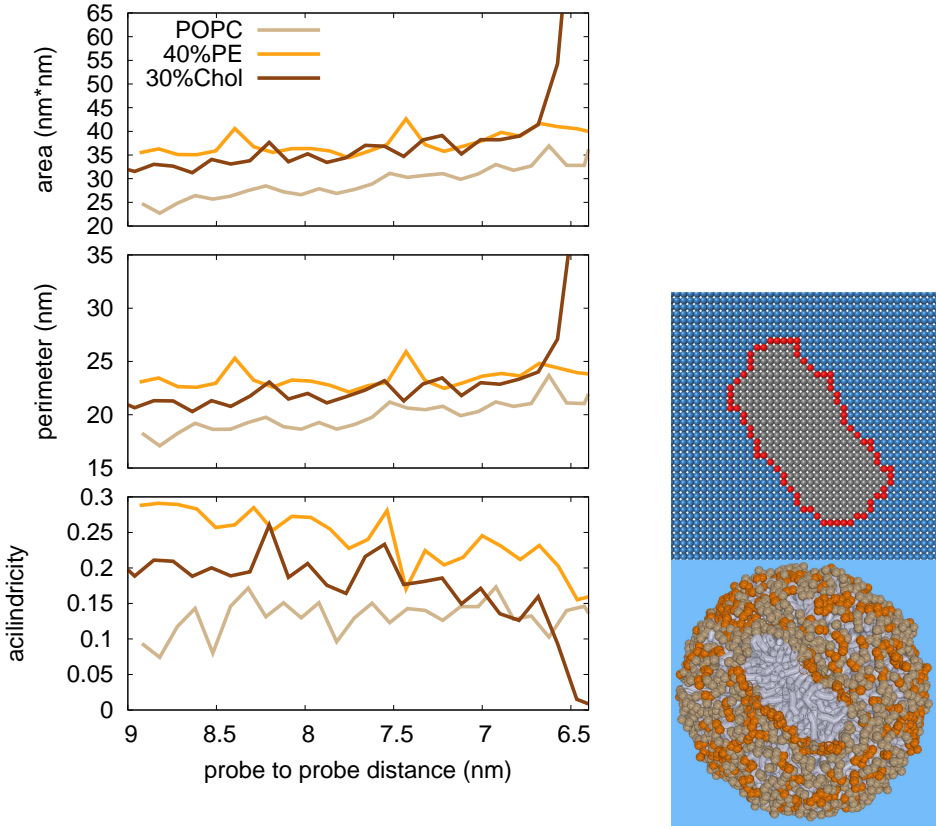


Figure 4: Average shape and size of the stalk at different stages along the reaction coordinate (stalk widening pathway). In these simulations flip-flop between the monolayers is present. The lines end at the point where the subsequent stalk widening becomes spontaneous (expansion barrier). Here, the stalk region is defined as the region within 1 nm above and below the stalk center (± 100 lipids). (*left panel*) The cross-sectional area, the total length of its circumference, and the acilindricity of the stalk. The acilindricity is a measure of how much the shape of the stalk deviates from radial symmetry, it is 0 for a perfect circle and 1 for an infinite thin rod/line. In all three membrane systems the stalk is rather asymmetric in the relaxed state. The presence of 40% POPE or 30% Cholesterol increases the overall size of the stalk (area and perimeter), as well as the asymmetry. Formation of the hemifusion diaphragm is characterized by a drop in acilindricity, i.e. the stalk is becoming radially symmetric, and sudden increase in area/perimeter. (*right panel*) Algorithm used to quantify the area, perimeter, and acilindricity. For the cross-sectional image of the stalk we only included the lipid beads (carbon-tails and glycerol groups) that are within 0.5 nm distance from the central plane through the stalk. This cross-sectional 'image' was mapped (using an overlap radius of 0.3 nm for each bead) onto a grid where each grid size had a dimension, $A_{grid} = 0.28 \times 0.28$ nm. The stalk was subsequently identified by a cluster algorithm. Here, two grid elements belong to one cluster if one of their four sides are directly contacting. Within such a definition, the stalk perimeter is a cluster element that has 3 or less direct contacts. Now, the area of the stalk is given by $N_{stalk} * A_{grid}$ and the perimeter length is approximated by $N_{perimeter} * \sqrt{A_{grid}}$. The acilindricity is defined as $\frac{(\lambda_x - \lambda_y)^2}{(\lambda_x + \lambda_y)^2}$, where λ_x, λ_y are the principal axis of the gyration tensor composed of all stalk perimeter elements.

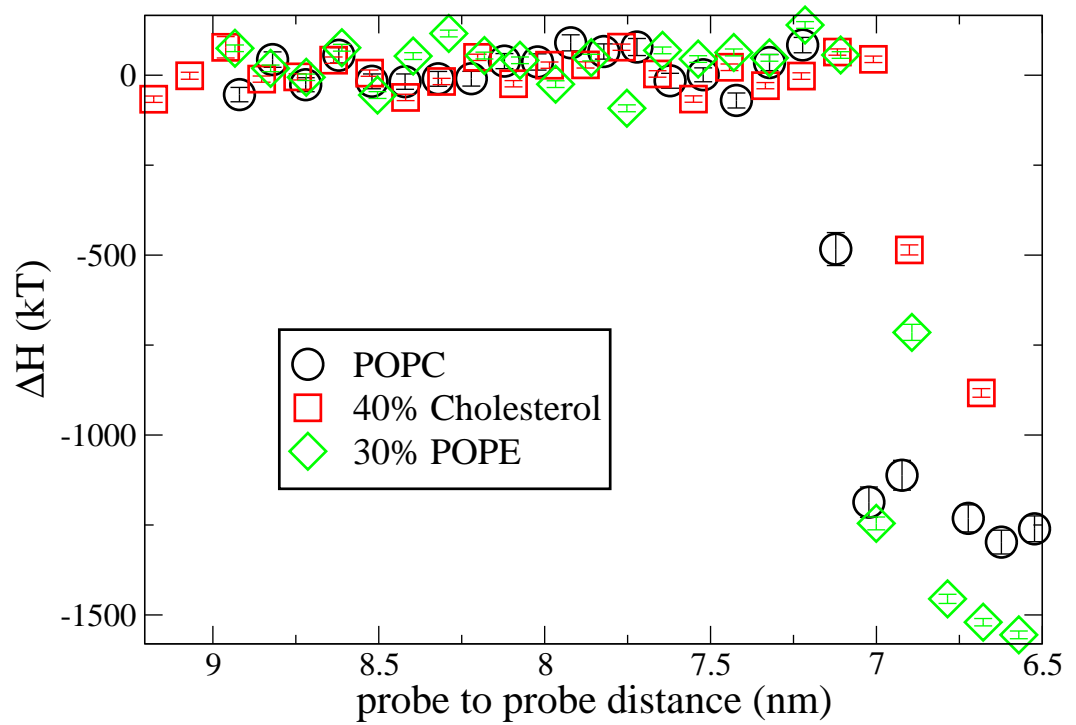


Figure 5: Relative change in enthalpy during stalk widening. The enthalpy remains apparently constant until the barrier against stalk expansion is surpassed. The latter is characterized by a strong drop in enthalpy, i.e. the subsequent expansion of the stalk is enthalpically favorable.

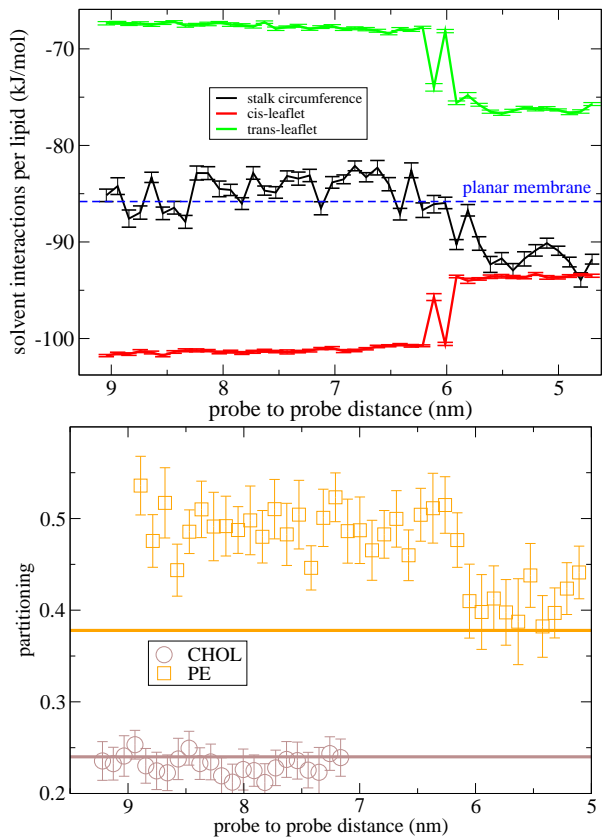


Figure 6: Hydration and composition of the stalk’s circumference at the different stages of stalk widening. Here, the stalk region is defined as the region within 1 nm above and below the stalk center (± 100 lipids). (figure above) Lipid-solvent interactions in the stalk and membrane leaflets elsewhere (pure POPC). The (negatively curved) cis-leaflets of the dimple/vesicle show a pronounced decrease in lipid-solvent interaction energy. Note that the \square -shaped circumference of the stalk becomes less negatively curved, and thus more hydrated, when formed between two dimples as opposed to two planar membranes. Infact, the lipids in such a shallow stalk are similarly hydrated as lipids in the corresponding, fully hydrated planar membrane. Because lipid head-group hydration does not come from the ‘bottleneck’ in such a stalk widening, the addition of, for example, POPE lipids is not expected to enhance stalk widening. Moreover, widening of such a dimple stalk increases head-group hydration. (figure below) Partitioning of POPE (40%) and Cholesterol (30%) in the stalk region (cis-leaflets) for different umbrella windows. The solid lines depicts the overall concentration in the (outer) cis-leaflets of the equilibrated, relaxed hemifused vesicle/dimple. The error bar gives the standard deviation of the average. We note that the (outer) cis-leaflets are depleted in cholesterol and PE – these components preferably partition in the (inner) trans-leaflet of the dimple. A pronounced increase in partitioning is observed for POPE, but not for cholesterol. It should be noted that the composition of cholesterol elsewhere in the cis-leaflets can not be exactly defined as about 5% of the total cholesterol content resides in the middle of the membrane. The sudden transition in stalk partitioning (POPE) is due to the formation/expansion of the HD.

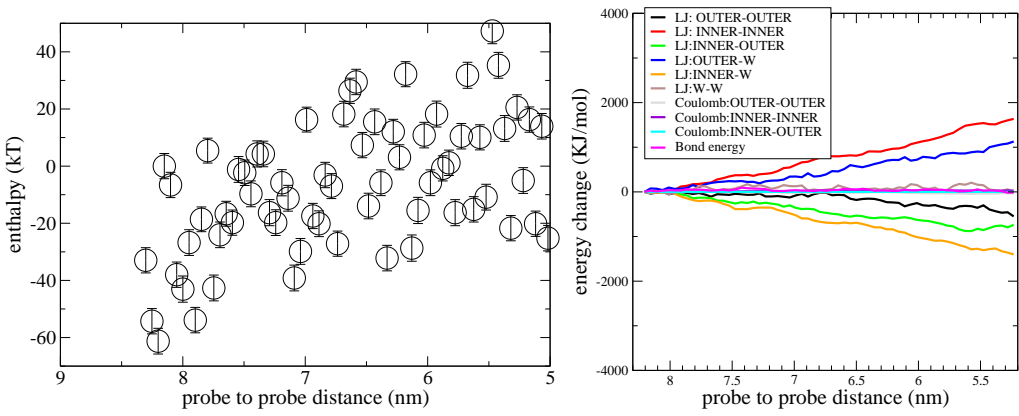


Figure 7: Enthalpy and enthalpy decomposition of stalk widening for the unequilibrated, asymmetric vesicle/dimple (artificial pores are not present). The barrier against stalk widening is about $50 k_B T$. The here obtained vesicle has 1447 lipids in the (outer) cis-leaflet and 770 lipids in the inner trans-leaflet versus the equilibrated vesicle which has 1414 and 803 lipids respectively. Thus, 33 lipids more in the outer leaflet (2.3%) and 33 lipids less in the inner leaflet (4.1%). (*left panel*) In contrast to the equilibrated vesicles/dimples (Fig. S2), widening of the stalk prior to barrier crossing is associated with an enthalpic cost. (*right panel*) Corresponding energy decomposition. Stalk widening is mainly opposed by a decrease of lipid-lipid interactions in the trans-leaflets, i.e. additional stretching of the trans-leaflets.

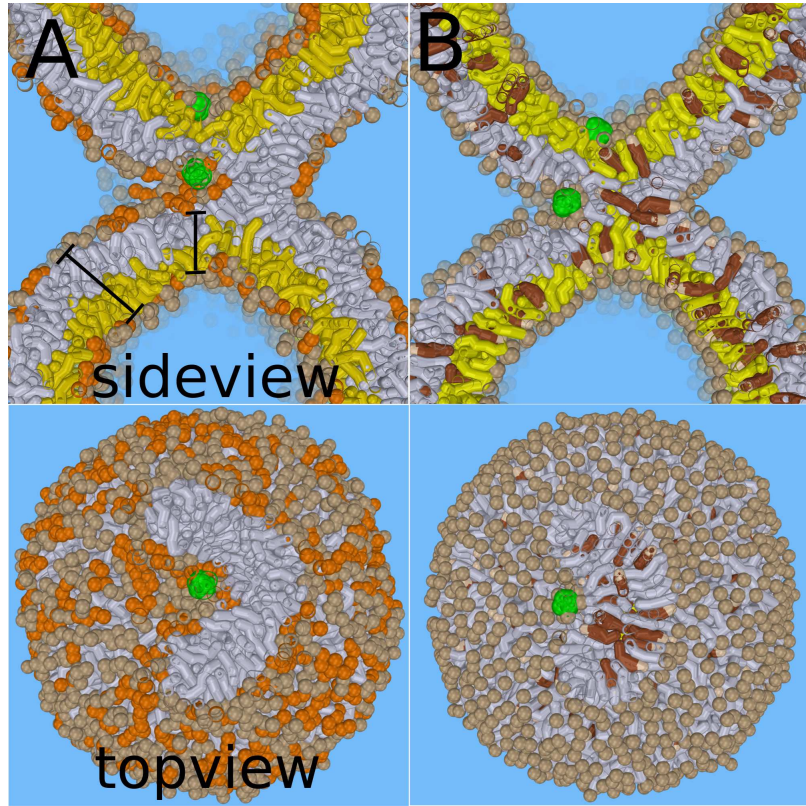


Figure 8: Leaky stalk expansion in the mixed membrane systems in close vicinity of the barrier. (A) 40% POPE (orange color). Probe to probe distance is 3.3 nm. The black bars indicate the membrane thinning of the encircled membrane regions. The stalk encircles the membrane perturbation prior to leakage pore formation. We emphasize that inverted hexagonal phase forming components, such as POPE and cholesterol lipids, are expected to enhance stalk elongation, i.e., formation of a four-bilayer junction (Katsov et al., Biophys. J., 2006). The circular elongation of the stalk enhances pore nucleation because the (partly) encircled membrane regions are subjected to an additional stress. This stress is reflected by the reduction of membrane thickness in the early hemifusion diaphragm(s). (B) 30% Cholesterol (brown color). Probe to probe distance is 1.8 nm. The increased elastic moduli of the membrane opposes the ability of the elongated stalk to (strongly) bend and to encircle the membrane perturbation. This reduces the ability of the stalk to impose stress on the encircled membrane fraction. We note however that, cholesterol neither alters the elastic moduli, nor enhances lipid tail ordering, when both tails are unsaturated, such as for DOPC, and when the membranes are in the liquid disordered phase (Pan et al., Phys. Rev. E, 2009). Thus, the presence of these lipids likely reduces the ability of cholesterol to prevent leaky fusion.

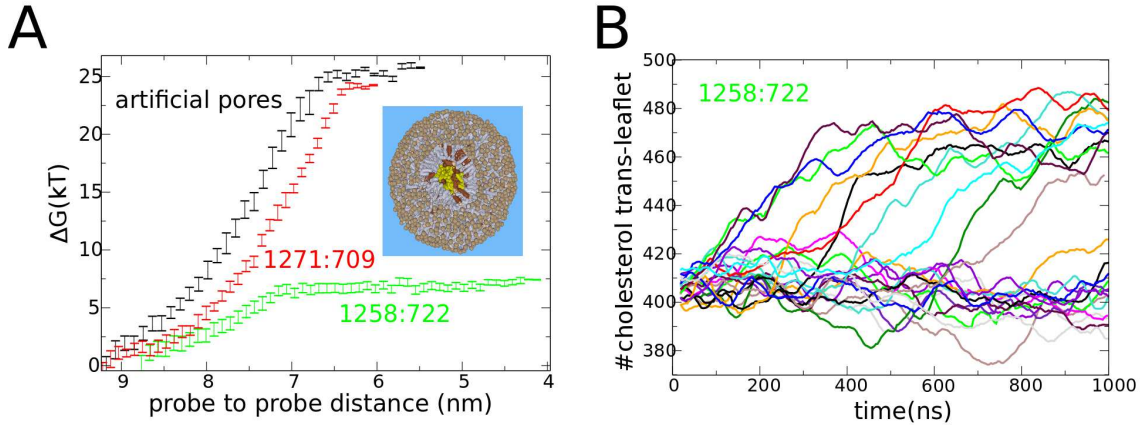


Figure 9: Widening of the stalk in the presence of 30% cholesterol. (A) The barrier against stalk widening is $25 k_B T$ for the equilibrated vesicle with artificial pores (black points). Removal of the pores after equilibration yields a similar barrier (red points). However, for a vesicle formed by spontaneous formation without additional equilibration (green point) the barrier is substantially reduced to about $8 k_B T$. The equilibrated vesicle has 1271 POPC lipids in the trans-leaflet and 709 in the cis-leaflet. In contrast, the 'non-equilibrated' vesicle has 1258 POPC lipids in the trans-leaflet and 722 in the cis-leaflet. Although, cholesterol can freely redistribute itself over the leaflets it does not compensate the effect of excess PC material in the trans-leaflet. We emphasize that membrane curvature and leaflet compositions are coupled. Because POPC is unable to flip-flop within the time scale of the simulation the leaflets can not adapt the preferred POPC:Cholesterol composition at the given leaflet curvature. (B) Flip-flop of cholesterol for each umbrella window in the 'non-equilibrated' vesicle. Cholesterol is able to sufficiently flip-flop within the time scale of the simulations. The strong increase in cholesterol content indicates that the HD has formed.

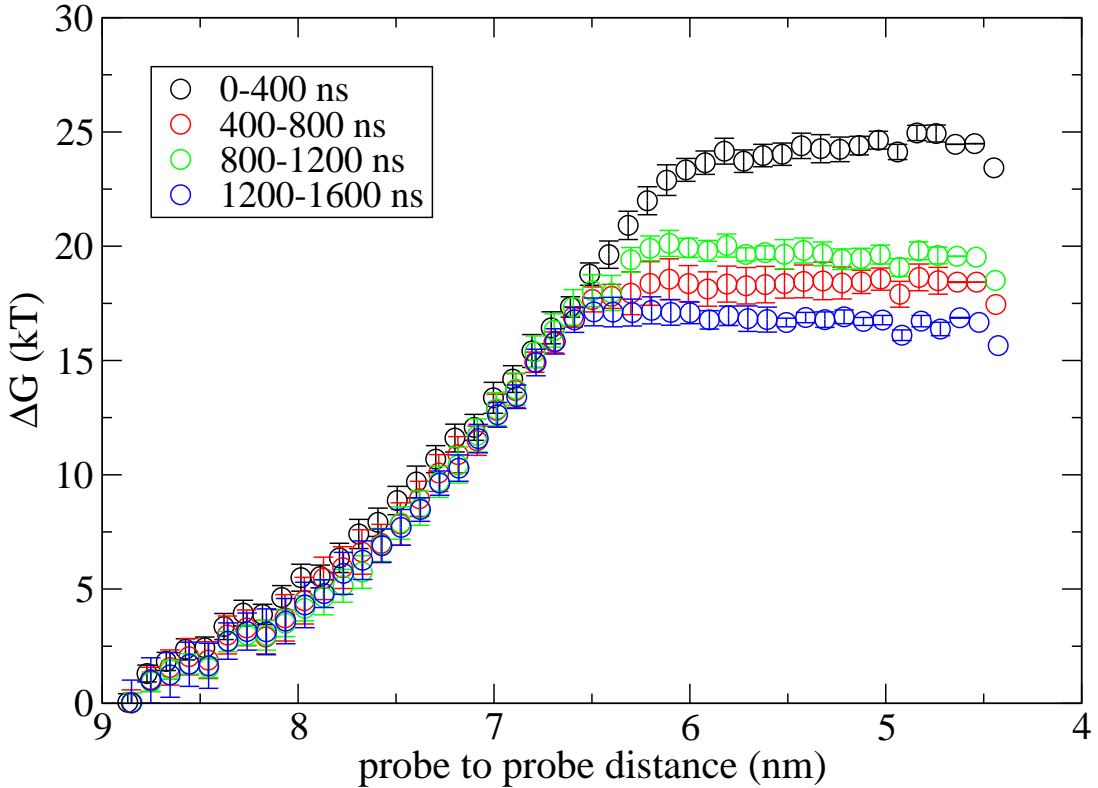


Figure 10: Free-energy derived for different time intervals. In our simulations we bring the system close to its barrier such that barrier crossing (nucleation) can occur within the 1.6 microsecond time-scale of the umbrella simulations. After nucleation the force on the probes vanishes. The plateau in the plot indicates the presence of such a nucleation in the simulation. In order to estimate the underlying free energy barrier, the simulations should be sufficiently short such that nucleation along the reaction coordinate becomes unlikely if the remaining free energy barrier is larger than several $k_b T$. For example, if the umbrella simulations would be infinitely long, barrier crossing eventually occurs everywhere along the reaction coordinate and no apparent free-energy barrier would be measured. On the other-hand, however, the simulations should be sufficiently long in order to allow the membrane to adapt to the decreasing probe to probe distance (equilibrated pulling forces). We consider the first 400 ns (black line) equilibration, and average the forces over 400-1600 ns.

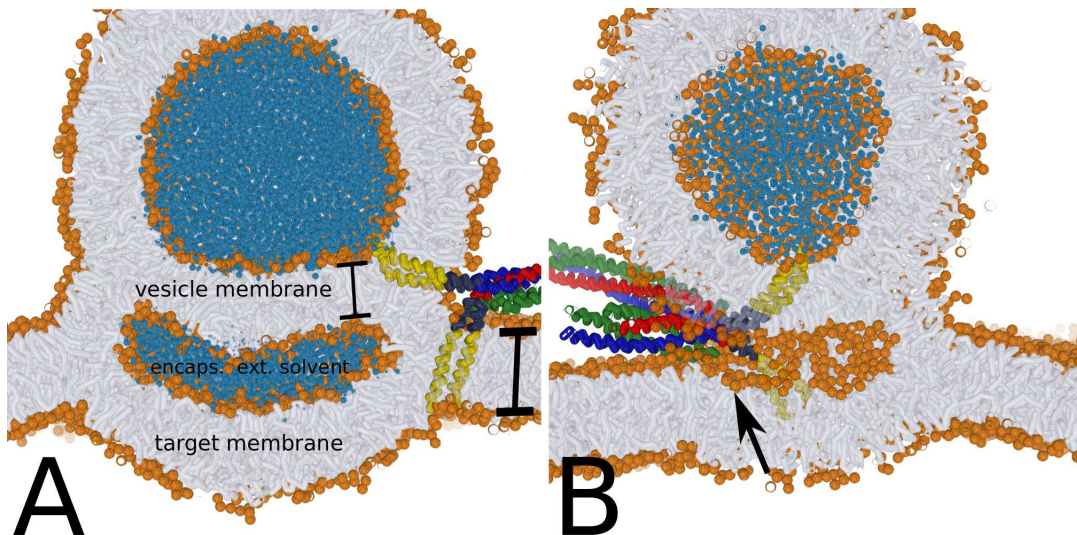


Figure 11: Alternative pathways. (A) Example of an double 'HD', i.e. an inverted micelle intermediate (IMI) formed in the reaction fusion between a bilayer and vesicle (For further details see Risselada et al., *Chem. Bio. Chem.*, 2011 and Risselada et al., *Curr. Opin. Struct Biol.*, 2012). When the stalk encircles the perimeter of the contact interface between the membranes (vertex ring), it encapsulates exterior solvent and forms a double 'HD'. The membrane(s) of the IMIs are under stress (black bars). This pathway can only occur when the expansion of the stalk via elongation is spontaneous and does not face a free-energy barrier. (B) IMI-pathways are leaky when the IMI would rupture before completion. The black arrow depicts the remaining opening in the IMI.

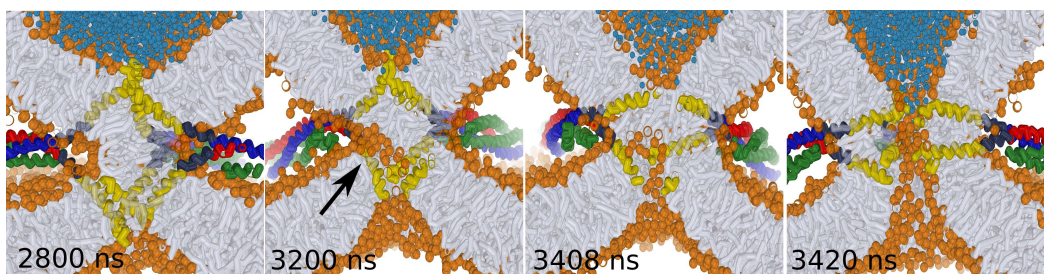


Figure 12: Fast leaky fusion. Example of a sub-microsecond leaky progression of the stalk in the SNARE-mediated fusion reaction between a vesicle and bilayer.

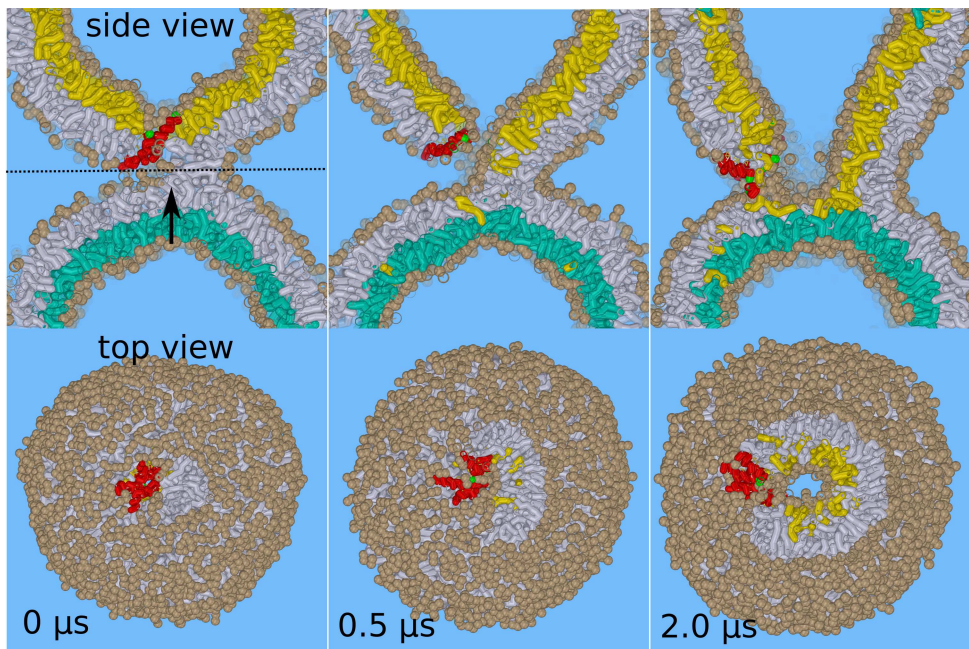


Figure 13: Leaky elongation of the stalk in the presence of five influenza fusion peptides (see Risselada et al., PLoS ONE, 2012 for further detail). To mimic the presence of the M1 protein matrix the bending of the cyan colored leaflet is retrained. The N-terminus of the peptide is colored green. The amphiphilic peptides favorably partition in the formed leakage pore which hinders 'closing' of the elongated stalk. This leaky intermediate displays a striking resemblance with the leaky intermediates formed in the fusion reaction between the influenza virus and liposomes observed in recent electron cryo-tomography studies (see Fig. 5B in Lee KK, Embo J., 2010). In these experiments, intermediates are studied by quenching the pH. When the pH is only partly increased the adhered M1 matrix remains stable and consequently stabilizes a formed HD. We emphasize that the metastability of such an leaky intermediate strongly relates to the survival of the HD (and thus the pH), because the leakage pore closes when the HD ruptures (see Fig. S4 in Risselada et al., Plos One, 2012). Therefore, the experimentally observed metastable intermediate likely occurs due to 'quenching' of the fusion reaction rather than 'misguidance'.

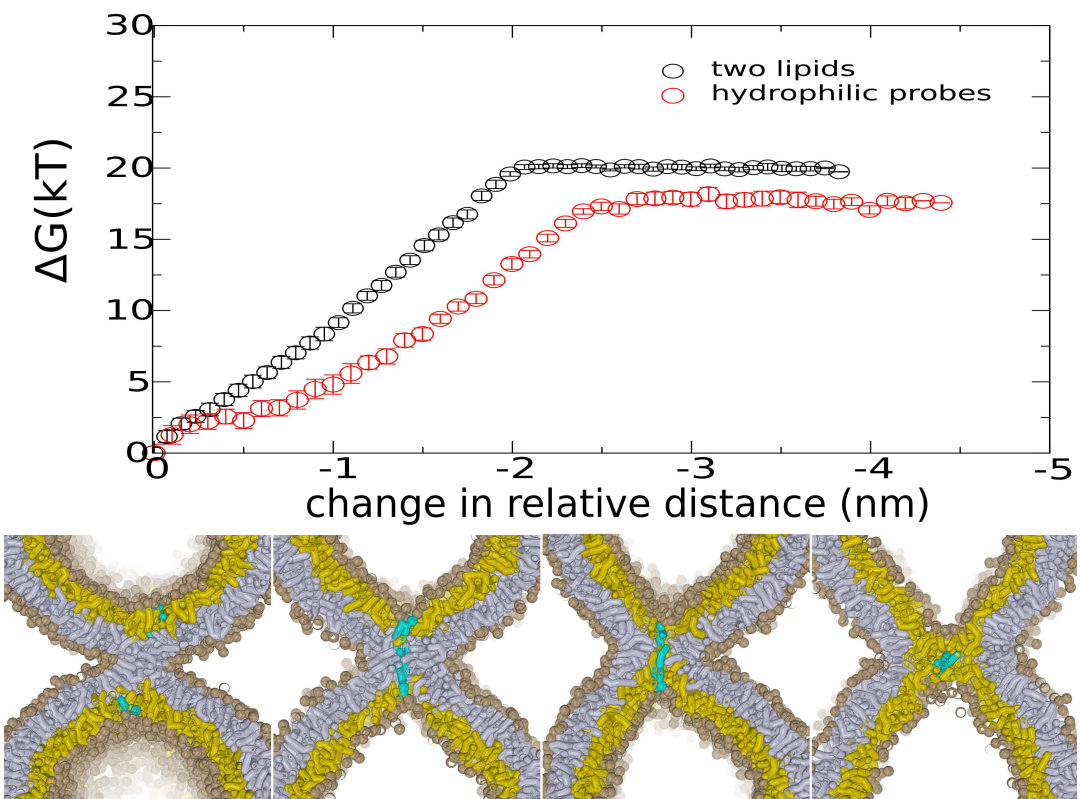


Figure 14: Enforcing stalk widening by pulling two lipids rather than two probes. The obtained barrier against stalk widening is 18 $k_b T$ (probes) versus 20 $k_b T$ (lipid), and thus rather independent on the local interaction between the probe and the lipids.

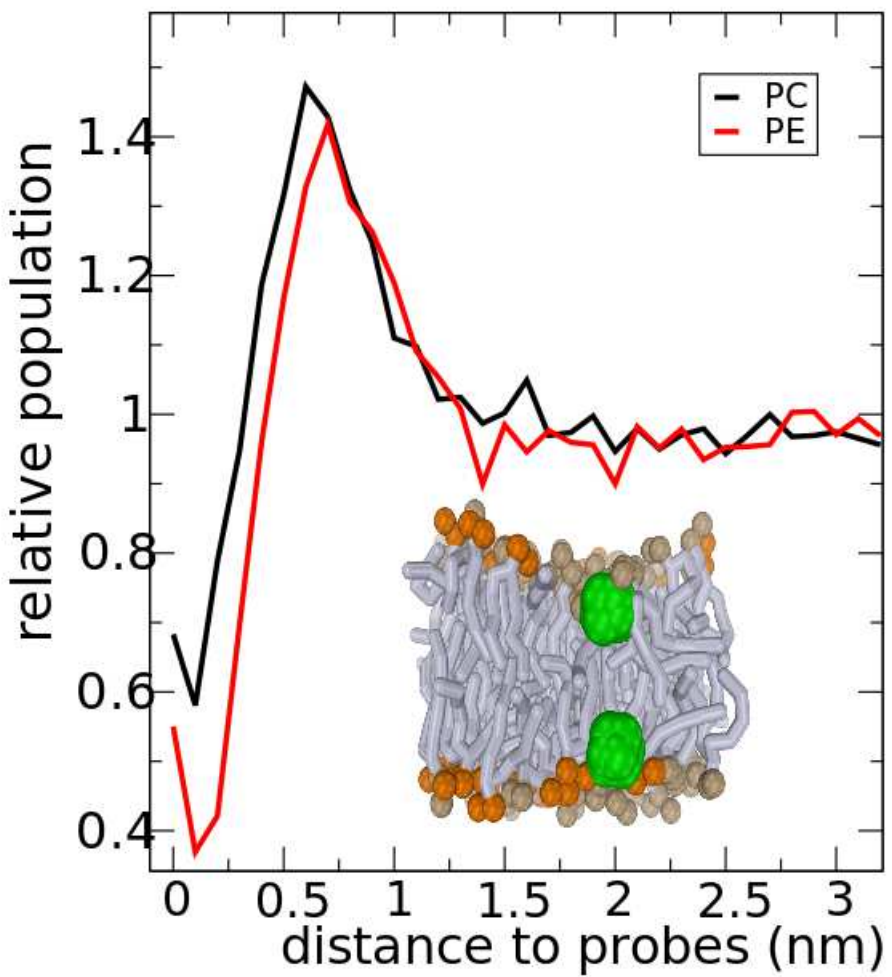


Figure 15: Interaction between the hydrophilic probes and lipid headgroups in a mixed POPC:POPE membrane (40% POPE). Shown is the normalized radial distribution function (calculated only within the membrane plane) of the lipid head groups with respect to the hydrophilic probes. The probe to probe distance is 2.5 nm and the probes subject a substantial squeezing force on the membrane. The plot illustrates that the presence of the probes hardly affects the nearby membrane composition. The first peak in the radial distribution function corresponds to the most probable distance between the probes and lipid headgroups, and relates to their geometrical dimensions. The slightly increased attraction between the probes and PC headgroups is explained by the increased hydrophilic nature of the PC headgroup with respect to the PE headgroup. Hence, the probes are comprised of solvent beads and are therefore slightly more attractive to PC headgroups than to PE headgroups.